Indian Journal of Engineering & Materials Sciences
Vol. 27, June 2020, pp. 518-528

Nanohardness and wear behaviour of AISI 1040 steel coated with Ti-6Al-4V $4B_4C$ by magnetron sputtering

Malkiya Rasalin Prince Russel[a*] & Selvakumar Natarajan[b]

[a]Department of Mechanical Engineering, Karunya Institute of Technology and Sciences, Coimbatore - 641114, Tamilnadu, India

[b]Department of Mechanical Engineering, Mepco Schlenk Engineering College, Sivakasi - 626005, Tamil Nadu, India

Received:14 June 2017 ; Accepted:20 February 2018

The Ti-6Al-4V-4B4C composite coatings have been deposited on AISI 1040 steel substrates by magnetron sputtering. The composition, structure, and topography of the coated surface have been explained by SEM, XRD, FT-IR and AFM. The constant coating thicknesses of 80 nm and 115 nm obtained for 0.5 h and 1h coating time, respectively. Wear tests have been conducted on the coated AISI 1040 steel substrates by using ball-on-disc apparatus under 2N and 3N loads at room temperature. The Ti-6Al-4V-4B4C coating has shown an excellent wear rate with a lower coefficient of friction. The nano-hardness and elastic modulus of the AISI 1040 steel coated with Ti-6Al-4V-4B4C has been attained by the AFM nano indentation technique that showed the maximum value of 10.7 GPa and 206.4 GPa, respectively. Ti-6Al-4V-4B4C composite coatings have displayed to lowest wear rates among all loading conditions, hence signifying that it could be a promising alternative to other hard coatings.

Keywords: Sputtering, Nanoindentation, Ball on discwear, Ti-6Al-4V-$4B_4C$

1 Introduction

Physical vapor deposition (PVD) was one of the oldest techniques used for the preparation of hard coatings[1]. Thin film coatings are the most common technique used for tribological purposes, since no post-deposition processing is required[2]. Carbide and nitride coatings improve the wear resistance, high strength and better hardness of products[3]. Wear resistance of AlCrN coating gives high abrasion resistance, better oxidation resistance and reasonable thermal stability[4].The metal nitrides and carbides with high hardness play important role in surface engineering field[5]. Hardest metal carbide coated stainless steel components shows outstanding properties[6]. Nanoindentation technique is an assessable method to evaluate the mechanical properties of thin film coatings. The XRD, SEM and AFM applied to characterize the surface topography of thin film coatings[7, 8].The surface roughness of the thin film coating has been investigated by using AFM image analysis[9]. In general wear resistance of the metals can be improved with hard nitride and carbide coating, which exhibits better wear resistance, low frictional coefficient and improved hardness[10, 11]. Wear behaviour of CrCN coating shows lower coefficient of friction and better wear resistance[12]. The DLC coated 6150 steel substrates shows high nano hardness ranging from 18-19 GPa, because of the coating adhesion on the 6150 steel[13]. Ti-Al-Mo-N thin films show superhard properties (40 GPa), which cannot be recognized to leading high residual stresses alone[14].

Boron carbide was recommended protecting coating for tungsten tiles of ITER diverter. The thickness of the near graphite layer varies from 5 to 15 μm, and the overall coating thickness varied from 20 to 40 μm[15]. The nano-hardness and modulus value have been enhanced due to the introduction of boron carbide which shows maximum 16 and 195.2 GPa respectively. Friction tests were carried out against AISI 52100 steel ball by using ball-on-plate apparatus[16]. Boron carbide was a striking material for protective coatings of the cutting tools due to its higher hardness, elastic modulus. Nanoindentation technique was employed to measure the hardness and modulus. The maximum hardness of 29 GPa and elastic modulus of 247 GPa has been obtained[17]. Storage or transportation of spent nuclear fuel neutron absorber is used for safety purpose. B_4C/Al neutron radiation shielding has good mechanical property and thermal neutron absorbing ability[18].B_4C coating was deposited on silicon wafers by DC magnetron

*Corresponding author (E-mail: russelmecher@gmail.com)

sputtering technique. Wear tests and friction wear tester were executed to explore the tribological behaviors of the coatings at room temperature. It is noted that the coefficient of friction of the coating was reduced from 0.4 to 0.1, and wear resistance was improved from 0 to 1.2 vol.%. By adding aB_4C particle in the deposition process the coating exhibited the lowest friction and highest wear resistance[19].

Boron carbide is a robust material having high hardness, stability to ionizing radiation and most chemicals. Boron carbide coating has found a variety of applications, such as plasma-faced components in fusion reactors, electromagnetic radiation field, coatings on nozzles, high precision tooling dies, radiation shields for propulsion and space nuclear power systems and anti-corrosion coatings due to its greater physical and mechanical properties.

In this study, the microstructure, wear resistance and mechanical properties of DC magnetron sputtered AISI 1040 steel from a Ti-6Al-4V-4B_4C target were taken into consideration. The films were characterized by a wide range of techniques such as X-ray diffraction (XRD), Atomic force microscopy (AFM), Fourier Transform Infrared (FT-IR) and Scanning electron microscope (SEM). The mechanical and tribological properties were analyzed by nanoindentation and ball-on-disc apparatus, respectively.

2 Experimental Details

2.1 Materials

Titanium alloy Ti-6Al-4V has better mechanical properties at room temperature. Ti-6Al-4V has a low interstitial content that can be offered for particular applications, which demands superior ductility and fracture toughness. Boron Carbide is one of the hardest ceramic materials and standing third among the hard materials. General applications of Boron Carbide include the usage in tank armor, bullet proof vests, ceramic tooling dies, precision tool parts, evaporating boats for materials testing as well as various industrial applications. The raw powders of Ti, Al, V and B_4C provided by M/s. Sigma Aldrich (India) were used as target materials. Table 1 shows the chemical composition of AISI 1040 steel.

2.2 Substrate and Target Preparation

A solid Ti-6Al-4V-4B_4C target was prepared from Ti, Al, V and B_4C raw powders. The target with 50 mm diameter and 3 mm thickness was used for coating. Scanning electron microscope image of the pre-compacted Ti, Al, V and B_4C raw powders are shown in Fig. 1. Moreover raw powders exhibit an irregular, angular shape with rough surfaces.

The Ti-6Al-4V-4B_4C coating was deposited on polished AISI 1040 steel flat specimens with dimensions of 60 mm diameter and 3 mm thickness. The substrate was prepared by waterproof 350 grit silicon carbide grinding wheels followed by 60, 80, 120, 220, 320 grade Al_2O_3 waterproof papers. Moreover, n-propanol and acetone were used to remove the organic impurities. The cleaned substrates were used for coating. Prior to the coating, the residual contaminant was removed by argon ion bombardment for 30 min.

2.3 Ti-Al-V-B_4C Thin Film Coating Technique

Surface engineering is a multidisciplinary action to modify the properties of the surfaces of engineering components so that their utility and serviceability can be enhanced. Sputter deposition is a physical vapour deposition process for formulating thin films using a DC magnetron sputtering method. In this, the concerned material is released from a target (Ti-6Al-4V-4B_4C) and deposited onto a substrate (AISI 1040). Figure 2 shows the schematic representation of a magnetron sputtering system. The purity of the sputtering target material was around (99.9%) and the purity of the sputtering gas (Ar) was 99.99%. At the time of deposition process, the coating chamber was evacuated down to $1x10^{-5}$ bar; argon (Ar) gas was introduced and the substrates were blasted by argon

Table 1 — Chemical composition of AISI 1040 steel (wt. %) [20].

C	Si	Mn	S	P	Fe
0.35-0.44	0.20	0.75	0.05	0.04	98.52

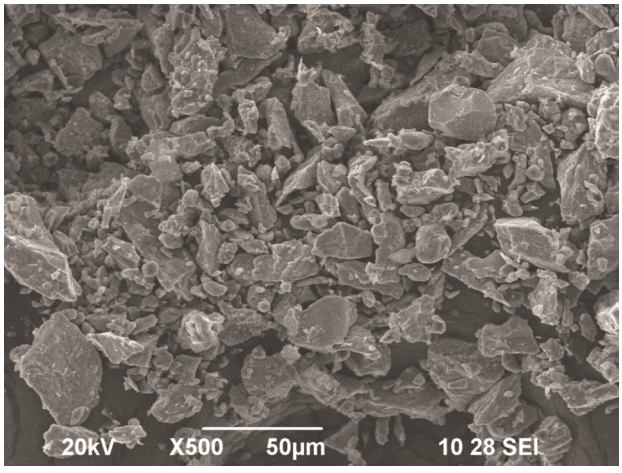

Fig. 1— SEM image of mixed powder Ti-6Al-4V-4B_4C.

ion (Ar+). The temperature of the substrate during the coating was maintained about 100 ± 20 °C. The coating time fixed for all specimens were 0.5 hand 1 h. Ti-6Al-4V-4B_4C adhesion layers were deposited on the substrate uniformly.

2.4 Characterization

2.4.1 AFM analysis

Atomic force microscope technique is suitable for attaining three-dimensional topographic information of thin film coatings. AFM nanoindentation measurement was executed to examine the mechanical properties of the coatings with the variation of loads by using AFM XE-70, Park Systems–S. Korea. The surface quality and roughness ofTi-6Al-4V-4B_4C coated surface have been obtained by statistical analysis of the AFM images. Z-scale of the AFM image shows the maximum and minimum heights of the features on the scanned area. AFM is equipped with a scanner range of 80 µm in the x and y directions and 10 µm in the z direction. Nano hardness of the Ti-6Al-4V-4B_4C thin film coating was calculated by performing force measurements on underlying AISI 1040 steel substrate at a sufficiently minor load to ensure little indentation.

2.4.2 XRD analysis

The crystalline structure of the Ti-6Al-4V-4B_4C coated AISI 1040 was assessed by using an XPERT-PRO diffractometer with Cu Kα radiation (k = 1.54060 Å), operating at 30 kV and 30 mA over the range of 2θ = 20–80° with a step size of 0.0170 and a step time of 3.1750 s. Peaks of the Ti-6Al-4V-4B_4C coatings were identified by using the X'Pert data viewer software[21]. The grain size and purity of the coating were determined by XRD analysis.

2.4.3 FT-IR analysis

The Fourier Transform Infrared (FT-IR) spectra were collected for ceramic nano coated AISI 1040 steel, using a Bruker Optics GmbH FTIR spectrometer, (Model: ALPHA, Germany). The functional groups of the Ti-6Al-4V-4B_4C coated AISI 1040 steel samples were recorded by using FT-IR. Spectra were obtained at 4 cm^{-1}resolution, with 24 numbers of scans on an average.

2.5 Wear Test

The ball on disc wear tester Ducom (Model: TR-20LE-PHM400) was used to conduct the dry sliding wear of Ti-6Al-4V-4B_4C coated AISI 1040 steel substrate shown in Fig. 3. Ti-6Al-4V-4B_4C coated samples were tested against E-52100 steel ball with 10 mm diameter and the hardness value of 450 VHN. The E-52100 steel ball counter body was pushed against the rotating wear sample with normal loads of 2N and 3N. Wear test was conducted at normal atmospheric temperature. The coefficient of friction was calculated based on the ratio between the friction force and the applied normal force. The mirror polished E-52100 steel ball was used with a surface roughness (R_a = 0.05 µm) for wear rate. The track radius of 20, 25, 30 and 35 mm were used for conducting the wear tests. The duration of wear test was fixed as 2 min. The loss of mass was weighed with an accuracy of ±0.01 mg by using a sensitive electronic balance. Further wear volume, sliding distance, wear rate, specific wear rate and coefficient of friction were calculated[22].

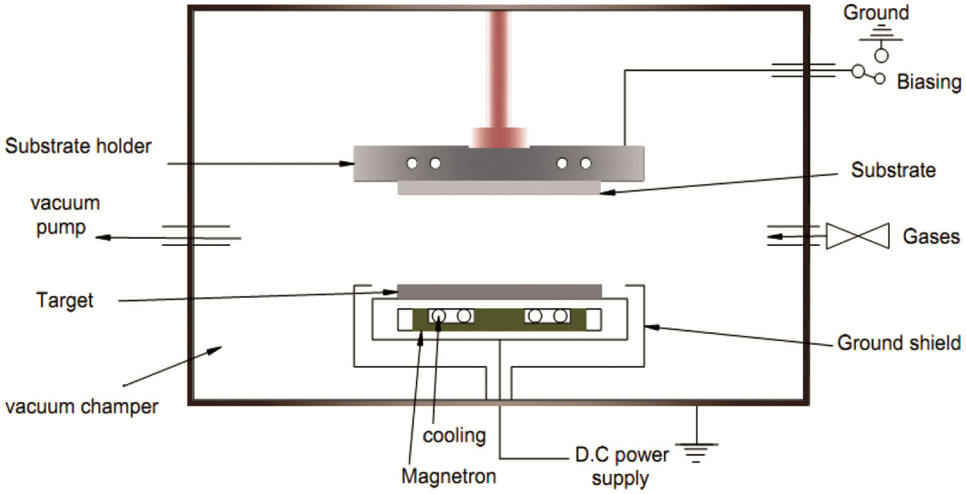

Fig. 2 — Schematic view of magnetron sputtering.

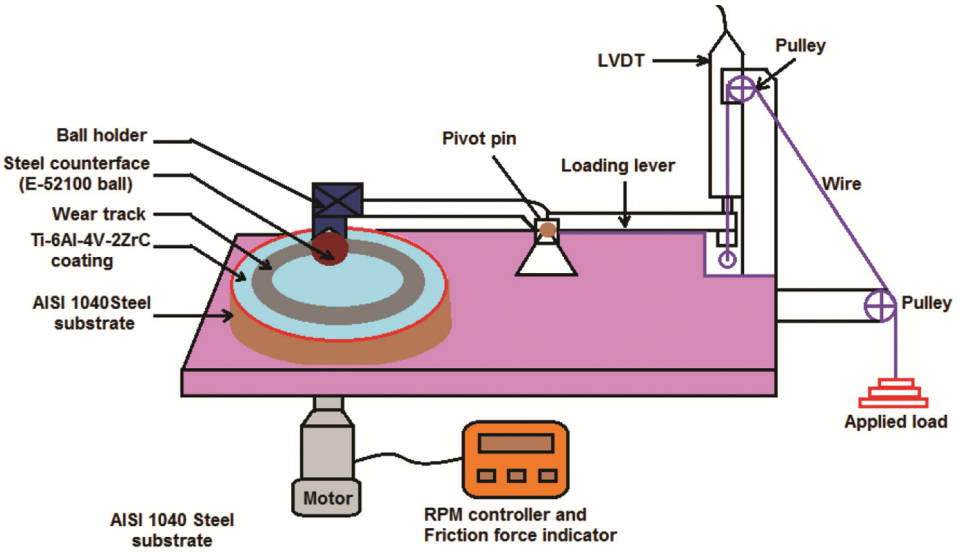

Fig. 3 — Schematic representation of ball-on- disc wear testing machine.

3 Results and Discussion

3.1 Surface Topography

The surface topography of the coating was analyzed by atomic force microscopy (XE 70, Park Systems–S. Korea). AFM technique is suitable for obtaining surface topography of thin film coatings in three-dimensions for structural analysis on the nanoscale.

Figure 4 represents the atomic force microscopy images of AISI 1040 steel substrate coated with Ti-6Al-4V-4B_4Cthin films at various time durations. From the AFM measurements, the root means square (RMS) roughness and film thickness were obtained. In Fig. 4, at the bottom side of the images, an intensity strip is shown, which indicates the depth and height along the z-axis. It is clearly shown that the thickness of the Ti-6Al-4V-4B_4Cfilm is increased with the deposition time. The AFM images show that there is large number of grains on the film surface which indicates that the grain size is progressively smaller. It is well known that AFM is one of the effective ways for the surface analysis due to its better resolution and powerful analysis. The growth of thin films was found to be irregular. It is observed that there is an irregular growth of grains due to an incomplete nucleation step. Thus, the films consist of larger and smaller grain size. The grains were packed very closely and showed a granular topography. The root means square roughness and thickness of the thin films were investigated using AFM images. Root mean square roughness is defined as the standard deviation of the surface height profile from the average height. The surface roughness of the film is unavoidable since grains were grown with different sizes and spherical in shapes. It can be observed that the films are uniform, well defined, spherical and cover the substrate well. These thin films reveal that there is an increase in the intensity of peaks which indicates a better crystalline phase in the films deposited on AISI 1040 steel. The addition of B_4C in coating causes a significant reduction of surface roughness. The surface roughness has been increased due to the increase in B_4C content and constant substrate temperature. Nano-particles were agglomerated into clusters easily during coating due to their smaller size and high surface energy. The B_4C nano-particles in the coating were agglomerated into clusters of few hundred nanometers size during the deposition process. It is observed that surface roughness of coating increases with increased B_4C particles. This is due to the formation of more B_4C particles in the coating that admits the formation of coarse structures which leads to increase the surface roughness. The higher surface roughness of Ti-6Al-4V-4B_4C thin film coating is due to the finer surface topography, more dense structure and also as a result of homogeneous distribution of nano B_4C particles in the coating. Moreover, the values of the roughness parameters, kurtosis and skewness also indicate that the surface of Ti-6Al-4V-4B_4Cthin films in contrast to reproduce the character of the surface of AISI 1040 steel substrate. It is noted that these films are uniform, regular, homogeneous and without any cracks.

Figure 4 (a) shows the surface topography of Ti-6Al-4V-4B_4C films with 0.5 h coating duration. From

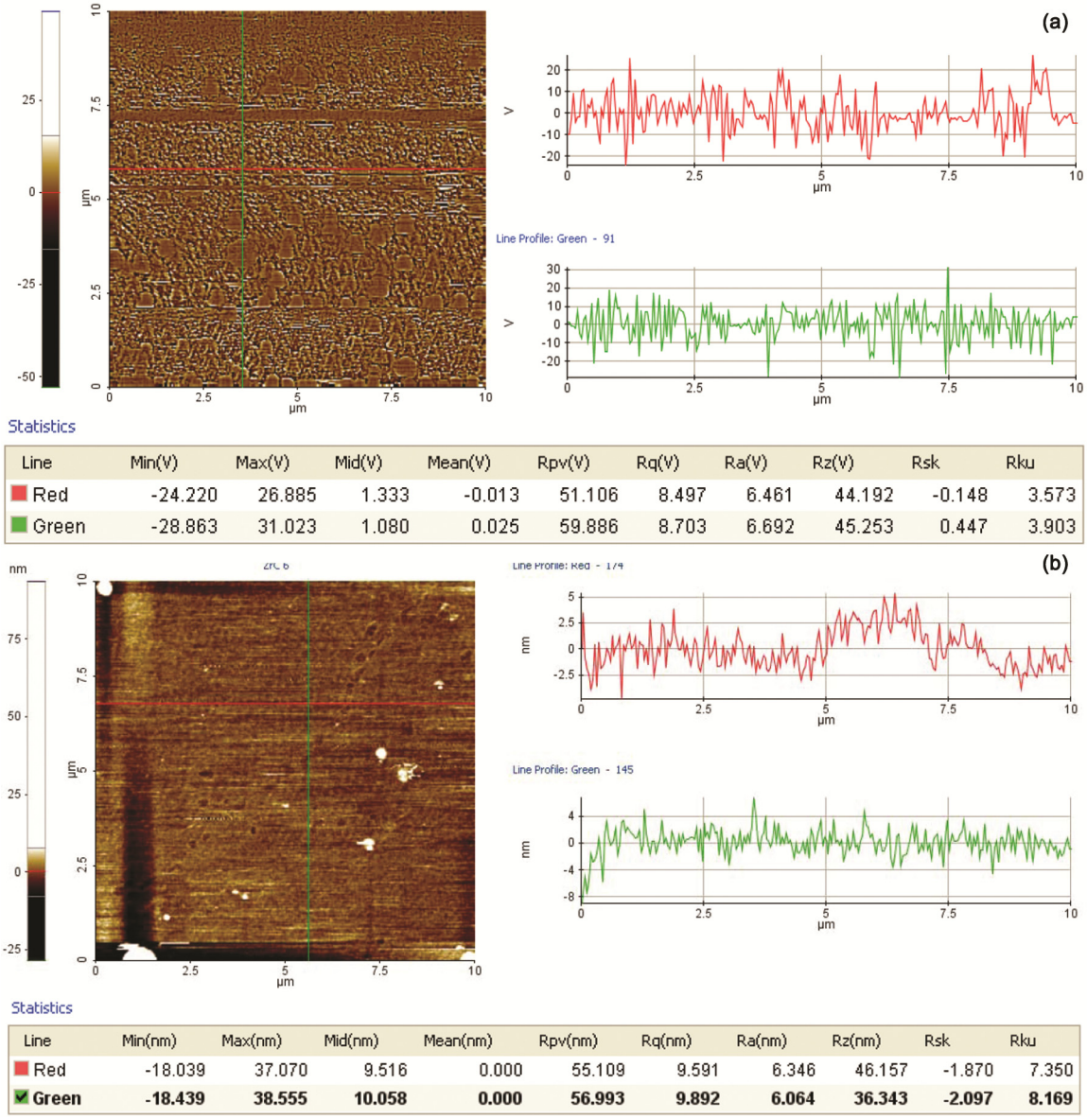

Fig. 4 — Topography of Ti-6Al-4V-4B_4C film (a) 0.5h coated and (b) 1h coated.

the AFM image, the root means square roughness (R_q) value, the surface roughness (R_a), coating thickness values, the average distance between the highest and lowest peak (R_z) were measured. It is clear that the coating thickness of the prepared film seems much thinner with a thickness of 80 nm. We obtained average surface roughness value from AFM image as 6.692 nm and average mean square value as 8.703 nm. The root means square of the Ti-6Al-4V-4B_4C coating and thickness of the film were investigated from AFM image. The three-dimensional AFM image displays the surface roughness of Ti-6Al-4V-4B_4C film with different grain sizes and shapes.

AFM image of the 1h coated Ti-6Al-4V-4B_4C is shown in Fig. 4 (b). The value of surface roughness, R_a, the average distance between the highest peak and the lowest valley, R_z, average mean square, R_q were found from AFM measurement. The thickness of the coating was obtained as 115nm. The surface roughness (R_a) of the Ti-6Al-4V-4B_4C coating was obtained as 6.064 nm, root mean square roughness (R_q) was achieved as 9.892 nm and averaged distance between the highest and lowest peak (R_z) was measured as 36.343 nm. The surface roughness, defects, amorphous and crystalline phases, and nucleation

and growth modes of the thin film can be evaluated from three-dimensional AFM image.

The obtained values of skewness (R_{sk}) and kurtosis (R_{ku}) were 0.447nm and 3.903nm respectively. Here both skewness (R_{sk}) and kurtosis (R_{ku}) were greater than zero. From the AFM measurements it was obtained that the Ti-6Al-4V-4B_4C thin film coated surface contains many peaks for0.5 h coating. For 1 h coating, the attained value of skewness (R_{sk}) and kurtosis (R_{ku}) were 2.097 nm and 8.169 nm, respectively. As per the AFM measurement, it was observed that the coated surface contains valleys and the results strongly insist that the coating time controls the surface roughness of the coating.

3.2 XRD Analysis of Nanocomposite

An X-ray diffraction spectrum, in 2θ geometry was carried out with monochromated Cu Kα radiation. X-ray diffraction (XRD) arrays of the Ti-6Al-4V with different 4% of B_4C particles are shown in Fig. 5. Ti, Al, V and B_4C peaks are noted in Fig. 5. Figure 5 shows Ti with a peak at 35.1°, indicating a strong (1 0 0) orientation in the coating using JCPDS file 89-2762.Moreover Ti peaks with 2θ values of40.2°, 62.9°, 70.6°, 76.1°and 77.3° belong to the crystal planes of (1 0 1), (1 1 0), (1 0 3), (1 1 2) and (2 0 1) respectively.2θ values of 38.4°, 44.8°and 78.3° peaks in the plane(1 1 1), (2 0 0) and (3 1 1) were confirmed using the JCPDS file no. 89-4037 for aluminium. For vanadium the characteristic peaks in the plane (1 1 0) can be matched with JCPDS file no. 65-6689 with a 2θ value of42.1°. The presence of boron carbide in the coating was represented in characteristic peaks in the plane of (2 0 0), (2 1 4) and (0 2 7) with 2θ values of 53.4°, 58.8°and 65.1° and it was confirmed using the JCPDS file No. 75-0424.The XRD analysis confirmed the purity of the Ti-6Al-4V-4B_4C coating, it was noted that no oxide peak was observed in the XRD analysis. This suggested that no intermetallic layer was found during coating and B_4C particles were stable during coating time. Moreover, the diffraction peaks in the XRD pattern are very sharp with the high intensity (Fig. 4) indicating the significant increase in grain size. In contrast, the broadening of these diffraction peaks indicates that the samples are smaller grain size. Based on the XRD patterns, all the peaks can be indexed to the cubic phase of Ti-6Al-4V-4B_4C and no impurity phase is detected.XRD patterns confirm the presence of B_4C in the coating. It is also noteworthy that the diffraction peaks of Ti, Al, V and B_4C have broadened. It confirms the presence of nano-sized particles in the coating. In the XRD pattern, the peak d001 corresponds to the d-spacing of the structure of Ti-6Al-4V-4B_4C, which can be calculated from Bragg's Law[23].

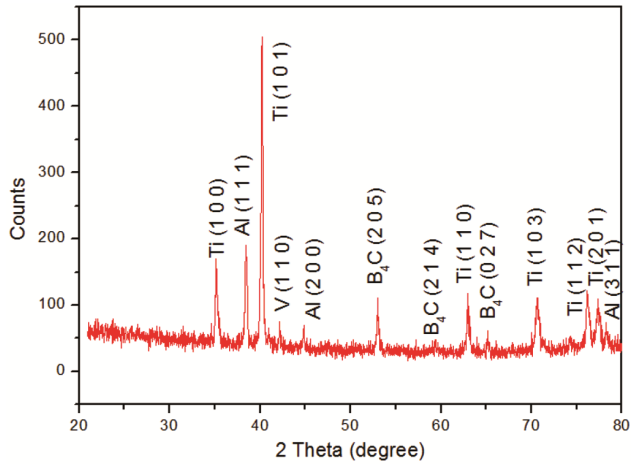

Fig. 5 — XRD pattern of the Ti-6Al-4V-4B_4C film coated on AISI 1040 steel.

3.3 FT-IR Spectroscopic Analysis

Infrared spectroscopy is used to determine the functional groups of molecules. IR Spectroscopy measures the vibrations of atoms, and based on the vibrations it is possible to determine the functional groups. In general, stronger bonds and lighter atoms will vibrate at a high stretching frequency. This method is based on the simple fact that, a chemical substance shows marked selective absorption in the infrared region. Figure 6 shows the details of the vibrational frequencies of Ti-6Al-4V-4B_4C coating recorded in the solid mode of the FT-IR spectrometer. The spikes come from the substrate. It can be seen that the presence of B_4C in the coating confirmed by FT-IR spectra, shows a strong and broad peak at 1058.83cm^{-1}. It can be seen that the FT-IR spectra of B_4C thin film have two strong absorption peaks; one located at 1058.83cm^{-1} and the other at 1511.87 cm^{-1}. The above peaks are attributed to the presence of B_4C in the coating[24]. Thus, FTIR images confirmed the presence of B_4Cin the coatings performed using magnetron sputtering process. Further, it confirms the purity of Ti, Al and V metals in Fig. 4, since it does not show any metal oxide peaks.

3.4 Nano Hardness

Nano hardness of the thin film coatings can be evaluated by AFM nanoindentation technique on a very small scale. Nano indentation method is accomplished by striking a small sinusoidal varying

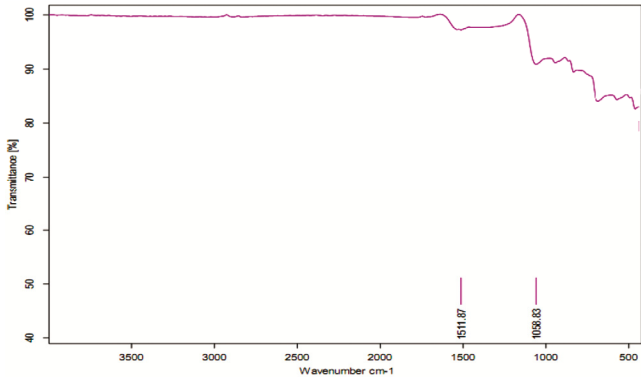

Fig. 6 — FT-IR spectra of Ti-6Al-4V-4B_4C coating.

force on top of the coating that controls the motion of the indenter. The penetration depth of the coating has been measured continuously from the movement response of the indenter at the maximum frequency and the phase angle between the force and displacement. The maximum force of 4 nN has been applied to the specimen for indentation. AFM probe with contact mode AFM can be applied to obtain the image of the coating. The force-displacement (F-D) curve was obtained during the indentation and nano-hardness of the coating has been obtained from F-D curve. The elastic displacements were recovered during the unloading time, and final depth of indentation was obtained. The nano-hardness is calculated by indentation load divided by the projected contact area[10]. The reduced elastic modulus of the coating has been determined based on the relations explained by Wei Hang[25].

Nanoindentation force-displacement curve of 0.5 h and 1 h coating time is represented in Fig. 7(a-b). Variations in surface topography also led to the scatter in measured values within 115 nm of the coating surface. The hardness and modulus values of Ti-6Al-4V-4B_4C coated AISI 1040 steel substrate for 0.5 hand 1 h were almost independent of indentation depths. In the two coatings, all data shows that maximum hardness and modulus values are about 10.7 GPa and 206.4 GPa. The nano-hardness and elastic modulus of Ti-6Al-4V-4B_4C coated AISI 1040 steel substrate for 0.5h and 1h increases gradually, due to the increase in coating thickness (range from 80 to 115 nm) and coating time. With the increasing coating time, the hardness and modulus curves begin to increase due to substrate effects. Clearly, it represents a composite property, consisting of a contribution from the Ti-6Al-4V-4B_4C coated AISI 1040 steel. The contribution of the underlying softer

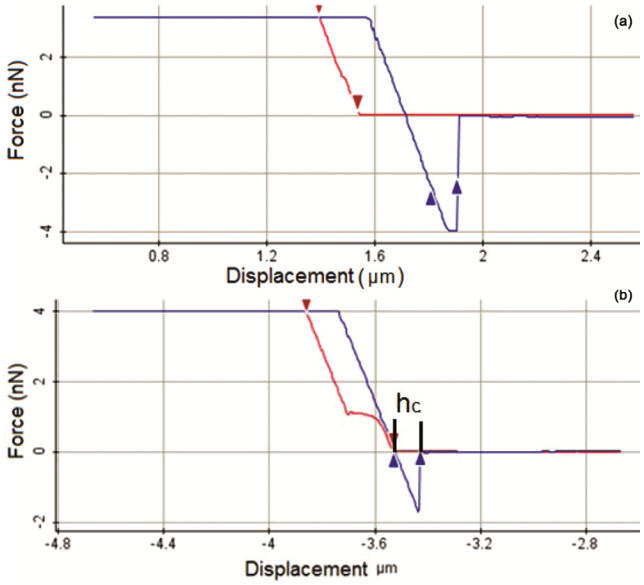

Fig. 7 — Nanoindentation force-displacement curve of coating (a) 0.5 h and (b) 1 h.

substrate with Ti-6Al-4V-4B_4C coating became more evident with a higher hardness.

Figure 8 shows the variation in nanohardness and elastic modulus ofTi-6Al-4V-4B_4C coating. The coating thickness has been increased due to the increase in coating time and constant substrate temperature. It is observed that nanohardness and elastic modulus of the coating increase with increased coating time. This is due to the more deposition time that admits the formation of coarse structures which leads to increase the nanohardness and elastic modulus. However, at higher coating thickness elastic modulus and nanohardness of the Ti-6Al-4V-4B_4C thin layers increases, moreover it is clearly stated that elastic modulus and nanohardness of Ti-6Al-4V-4B_4C coating increases with increase in the amount of B_4C reinforcement. The higher nano-hardness and elastic modulus of Ti-6Al-4V-4B_4C composite coatings are due to the finer surface topography, more dense structure and also as a result of homogeneous distribution of nano B_4C particles in the coating.

3.5 Wear Analysis

3.5.1 Dry sliding wear

The wear behaviour of Ti-6Al-4V-4B_4C thin film coated AISI 1040 steel against E-52100 steel ball was investigated. The wear test was conducted at normal atmospheric temperature. The sliding speeds are fixed at 0.5235, 0.6544, 0.7854 and 0.9163 m/s for wear tests with loads of 2N and 3N. The mass loss of

coated samples was about $0.2x10^{-4}$g, resulting in reduced wear rate of about 32 % when compared with mild steel substrate[26]. The reduced wear rate is generally due to higher hardness. In general brittle materials may have high wear rates as a significance of their inability to practice plastic deformation. Two main stages of wear were noted, first one is initial running wear and next one is steady state wear. The steady state coefficient of friction value of 0.44 was obtained, and that explains the nature of wear as steady state.

Figure 9 shows the specific wear rate of 0.5 h coating. The calculated values of specific wear rate are noted as 0.1013 x 10^{-5}mm^3/Nm to 0.1737 x 10^{-5}mm^3/Nm for 2N load. For 3N load the range of specific wear rate as 0.2027 x 10^{-5}mm^3/Nm to 0.2516 x 10^{-5}mm^3/Nm has arrived. It is clearly shown that there is no oxidization layer as there is no slitting of the coating during the wear test. The energy released due to the mechanical work leads to an increase in the temperature at the points of effective contact between counter body and coating. Even though, if the surface temperature of the sample increases due to frictional heat, some effects may occur, namely changes in mechanical properties and oxidation. The authors detected that wear rate of the Ti-6Al-4V-4B_4C coatings increased with increasing applied load and sliding distance. The wear loss of the coatings has been increased with increase in applied load and sliding distance. Moreover, presences of B_4C contents in the coating can reduce the wear rate of the coating, enhancing the hardness and reducing the frictional coefficient.

The wear behavior of Ti-6Al-4V-4B_4C coated AISI 1040 steel with 1 h coating time was investigated. The samples were tested against 2N and 3N loads. The average frictional coefficient was obtained in the range of 0.1 to 0.44 for all the tests. The transfer of Ti-6Al-4V-4B_4C film remains stable at the end of testing. The authors noted that the wear resistance of the coating increases with the addition of B_4C particles. Figure 10 clarifies the deviation of the specific wear rate with the 1h coating. The specific wear rate for 2N load was calculated from 0.1970 x 10^{-5}mm^3/Nm to 0.3297 x 10^{-5}mm^3/Nm and 0.3128 x 10^{-5}mm^3/Nm to 0.4472 x 10^{-5}mm^3/Nm with the 3N load. The authors report that the wear resistance of the Ti-6Al-4V-4B_4C coated AISI 1040 steel improved when compared with pure alloy. The wear loss of the coating has been increased linearly with the sliding distance for both 2 and 3N loads. It is clearly noted that the lower rate and low value of frictional coefficient have arrived. The higher coefficient of friction produces crack on the surface of the coating. Based on the whole results, low coefficient of friction with minimum mass loss has been achieved.

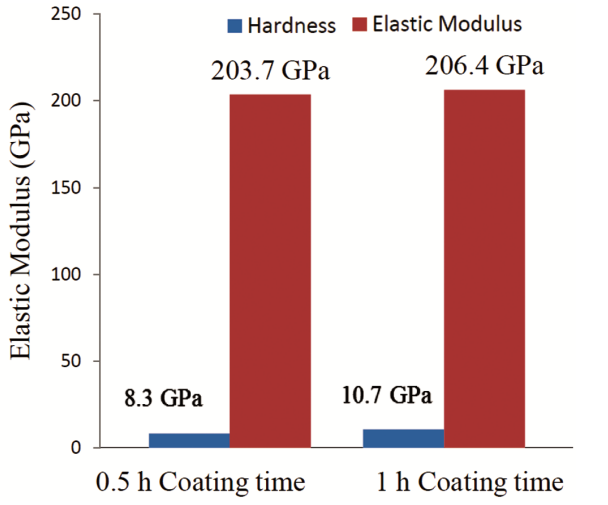

Fig. 8 — Variation of nanohardness and elastic modulus for various coating time.

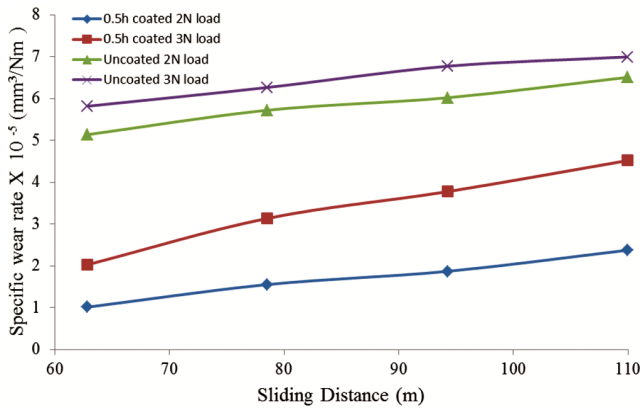

Fig. 9 — Specific wear rate of 0.5h coating.

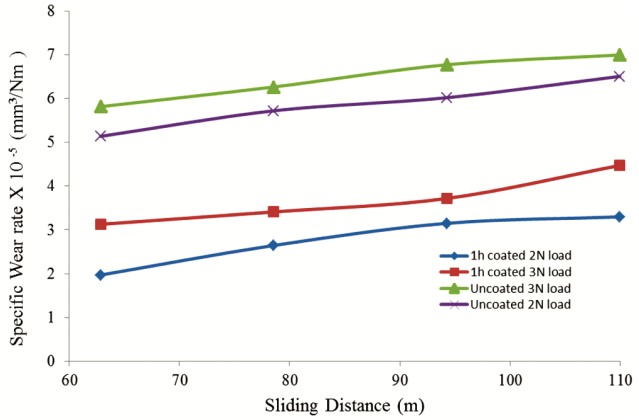

Fig. 10 — Specific wear rate of 1h coating.

Figure 11 shows the comparison of the specific wear rate with various wear testing time. The specific wear rate of the coating has been increased linearly with the time duration for both 2 and 3N loads. Under the same load condition, with an increase in time duration the rate of wear increases. In addition, no material transfer is observed on the worn Ti-6Al-6V-4B_4C layers under all test conditions. With the increase in sliding time the average wear rates and average wear volumes of AISI 52100 steel balls and Ti-6Al-6V-4B_4C coating surfaces increase up to the maximum value. The specific wear rate of Ti-6Al-4V-4B_4C coatings under dry sliding wear against E-52100 steel ball counter face is perceived to increase noticeably, at higher sliding distances. The amount of specific wear rate of Ti-6Al-4V-4B_4C coated AISI 1040 steel was decreased 14 % compared with uncoated AISI 1040 steel. This happens due to the presence of the carbon-rich particles on the coating surface which delivers higher hardness. The specific wear rate decreases with the addition of B_4C particle presence in the coating and also the specific wear rate for the coatings increases linearly with increasing applied load and sliding distance. The specific wear rates of both coatings increase with increasing sliding distances. Wear resistance is defined as the reciprocal of the weight loss of the coating for a given sliding distance. The specific wear rate of uncoated steel is higher compared with the Ti-6Al-4V-4B_4C coating. Maximum specific wear rate of uncoated steel shows 5.137 x $10^{-5}$$mm^3$/Nm for 0.5 h coating with maximum load and sliding distance has been obtained. Likewise, for 1h coating, the maximum specific wear rate of 7.0152 x $10^{-5}$$mm^3$/Nm has been obtained. Ti-6Al-4V-4B_4C coated AISI 1040 steel shows specific wear rate values up to 2 times lower than those of the uncoated AISI 1040 steel. The specific wear rate reduces the amount of B_4C reinforcement increases for all applied loads, but its effect is more predominant at minor loads. It is clearly specified that this parameter takes along the development in inherent wear resistance of the coating with an increase in the amount of B_4C reinforcement.

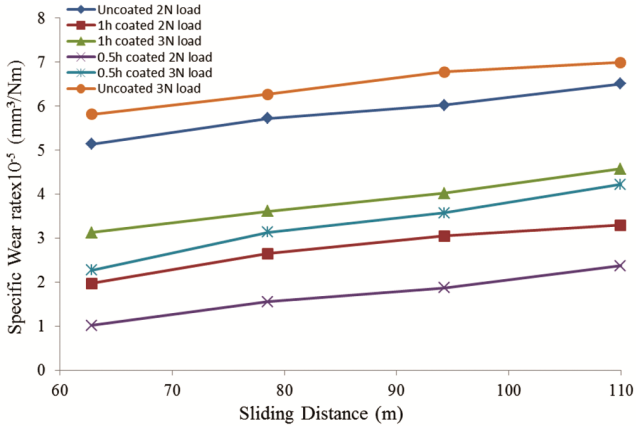

Fig.11 — Specific wear rate comparison.

3.5.2 Effect of counterface material

The friction and wear of the counter-body (E-52100 steel ball) were counted against Ti-6Al-4V-4B_4C coatings. E-52100 steel balls of diameter 10 mm with hardness about 62 Rc. Tests with these balls were conducted at room temperature over a time period of 2min. Figure 12 shows the deposition of coated particles on E-52100 steel ball. Figure 13 shows the variation of frictional coefficient during the test with E-52100 steel ball, sliding against Ti-6Al-4V-4B_4C coatings at 2N and 3N loads. In general,

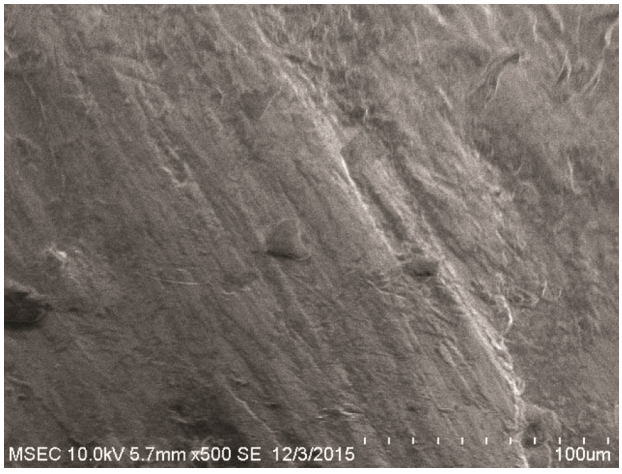

Fig. 12 — Coated material deposited on E-52100 steel ball.

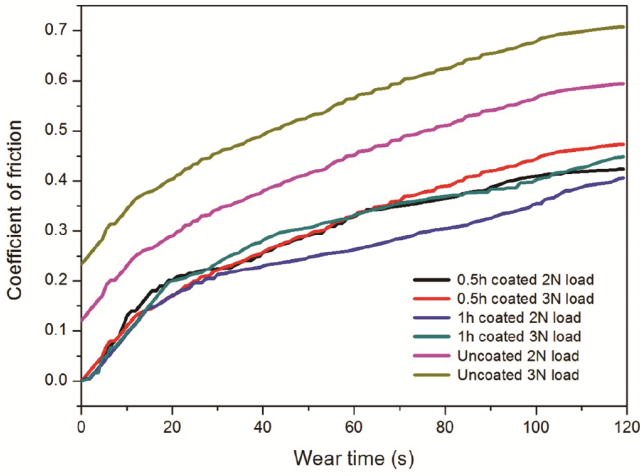

Fig. 13 — Friction behavior of Ti-6Al-4V-4B_4C coatings when sliding against E-52100 steel ball.

friction and wear of the counter-body depend upon the load, sliding distances and sliding speed conditions. The value of coefficient of friction started at comparatively low at 0.1, but progressively increased, finally ending with a final coefficient of friction value of about 0.42 and 0.47 for 2 and 3N loads with 0.5h coating time. The coefficient of friction increased with respect to sliding distance and time. While the Ti-6Al-4V-4B_4C coated AISI 1040 steel surface and counter-body (E-52100 steel ball) were in relative motion, the frictional heat developed between the surfaces were continuous because there was no time to dissipate the heat. Due to that reason the coefficient of was increased. Moreover, the steady coefficient of friction value for 1h coating has arrived as 0.40 and 0.44 against 2N and 3N load.

The hardness of the AISI 1040 steel has increased due to the increase of coating time and coating thickness. Additionally, the hardness increases with a decrease in coefficient of friction. Coefficients of friction attained for uncoated AISI 1040 steel is 0.6 for 2N load and 0.71 for 1h, 3N load. When compared with uncoated steel; coefficient of friction of Ti-6Al-4V-4B_4Ccoated AISI 1040 steel has been reduced by 80%. The value of the coefficient of friction is lower due to the several reasons: contact geometry, combination load and speed, better surface roughness, counter-body material, etc. Ti-6Al-4V-4B_4C coated AISI 1040steel suffers less amount of severe wear since it has a higher hardness. The high coefficient of friction and noise in the wear test data for the E-52100 steel ball was attributed to the broad transfers of metal from the coated surface. The behavior of the friction is the result of both transfer of material from E-52100 steel ball into the coating and the wear and damage of the coating. It is clearly noted that the value of coefficient of friction is lower than uncoated steel. The wear of the counter-body (E-52100 steel ball) was increased, due to the improvement of hardness on the coating. It seems that the hardness of the coating is comparatively higher than the counter body.

4 Conclusions

In the present work, nano-hardness, elastic modulus, thermal analysis, and wear analysis of the Ti-6Al-4V-4B_4C coatings were carried out with different coating times and loads. Based on the present experimental work, the following findings were made:

(i) Ti-6Al-4V-4B_4C coatings were characterized by AFM, FT-IR, XRD and the nature of coated surface looks like valleys explained by AFM. The XRD pattern shows the presence of Ti, Al, V and B_4C in the coating.

(ii) The AISI 1040 steel with Ti-6Al-4V-4B_4C coating was not ruptured up to 110 m sliding distance under the normal atmospheric test conditions.

(iii) The B_4C has a significant effect on the hardness and elastic modulus of 1h coating which produces maximum hardness of 10.7GPaand maximum elastic modulus of 206.4 GPa.

(iv) The values of coefficient of friction obtained lie in the range between 0.43 and 0.48 against 0.5h coatings and 0.42 and 0.45 against 1h coatings.

(v) Specific wear rate of Ti-6Al-4V-4B_4C coated AISI 1040 steel increases with increasing load and sliding distance.

(vi) When sliding against E-52100 steel ball counter body the Ti-6Al-4V-4B_4C composite coating showed significant enhancement in friction and wear resistance.

References

1 Wei H, Jiang X, Xiaolin L, Dongsheng H, Hongliang T, Paul M & Zong-Han X, *Appl Surf Sci,* 368 (2016) 177.

2 Lorenzo-Martin C, Ajayi O, Erdemir A, Fenske G R & Wei R, *Wear,* 302 (2013) 963.

3 Huiying Z, Yaran N, Chucheng L, Liping H, Heng J & Xuebin Z, *Ceram Int,* 39 (2013) 101.

4 Mo J L & Zhu M H, *Tribol Int,* 41 (2008) 1161.

5 Robinson G M & Jackson M J, *J Mater Process Tech,* 1 67 (2005) 316.

6 Chiccoa B, Borbidgeb W E & Summervillea E, *Mat Sci Eng A,* 266 (1999) 62.

7 Xia Y, Bigerelle M, Bouvier S, Iost A & Mazeran P E, *Tribol Int,* 82 (2015) 297.

8 Ozmetin A E, Sahin O, Ongun E & Kuru M, *J Alloy Compd,* 619 (2015) 262.

9 Sheng-Rui J, Guo-Ju C & Wei-Min H, *Mater,* 6 (2013) 4505.

10 Kailasanathan C & Selvakumar N, *Ceram Int,* 38 (2012) 3569.

11 Yu-Sen Y, Ting-Pin C & Han-Wen Y, *Surf Coat Tech*, 259 (2014) 141.

12 Hu P & Jiang B, *Vacuum,* 85 (2011) 994.

13 Silva V M, Trava-Airoldi V J & Chung Y W, *Surf Coat Tech,* 205 (2011) 3703.

14 Sergevnin V S, Blinkov I V, Volkhonskii A O, Belov D S, Kuznetsov D V, Gorshenkov M V & Skryleva E A, *Appl Surf Sci,* 388 (2016) 13.

15 Azizov E, Barsuk V, Begrambekov L, Buzhinsky O, Evsin A, Gordeev A, Grunin A, Klimov N, Kurnaev A,

Mazul I, Otroshchenko V, Putric A, Ya. Sadovskiy, Shigin P, Vergazov S & Zakharov A, *J Nucl Mater,* 463 (2015) 792.
16 Dongqing H, Lunlin S, Zhibin L, Guangan Z, Liping W & Qunji X, *Surf Coat Tech,* 329 (2017) 11.
17 Chen W, Yanqing Y, Yip-Wah C, Yingchun Z, Sheng O, Zhiyuan X, Kexin S & Pengtao L, *Ceram Int,* 42 (2015) 6342.
18 Peng Z, Yuli L, Wenxian W, Zhanping G & Baodong W, *J Nucl Mater*, 437 (2013) 350.
19 Ahna H S, Cuonga P D, Shinb K H & Ki-Seung L, *Wear*, 259 (2005) 807.
20 Salim S, *J Mater Process Tech,* 209 (2009) 1736.
21 Selvakumar N, Jinnah Sheik Mohamed M, Narayanasamy R & Venkateswarlu K, *Mater Design,* 52 (2013) 393.
22 Vettivel S C, Selvakumar N & Leema N, *Mater Des,* 45 (2013) 323.
23 Polychronopoulou K, Rebholz C, Baker M A, The odorou L, Demas N G, Hinder S J, Polycarpou A A, Doumanidis C C & Bobel K, *Diam Relat Mater,* 17 (2008) 2054.
24 Najafi A, Golestani-Fard F, Rezaie H R & Ehsani N, *Ceram Int,* 38 (2012) 3583.
25 Wei H, Libo Z, Jun S & Julong Y, *Precis Eng,* 37 (2013) 408.
26 Pereira D, Gandra J, Pamies-Teixeira J, Miranda R M & Vilaca P, *J Mater Process, Tech,* 214 (2014) 2858.